A HIERARCHICAL HYBRID ELECTRODE FOR RAPID OXYGEN REDUCTION REACTION BELOW 800 °C

by

Fushao LI[a,*], Yingxian XU[a], Shubiao XIA[a], Jianjun LIU[a], Yuxing YAN[a], Long JIANG[b], and Feixiang CHENG[a**]

[a] Chemical Functional Materials Research Center, Qujing Normal University, Qujing, Yunnan, China
[b] School of Physics and Optoelectronic Engineering, Yangtze University, Jingzhou, Hubei, China

Original scientific paper
https://doi.org/10.2298/TSCI2004455L

The 3-D backbones with ionic conductivity are first built by sintering $Ce_{0.8}Sm_{0.2}O_{1.9}$ silks, then $Ca_3Co_2O_6$ nanoparticles as electrocatalyst are filled in by infiltrating ionic solution, as a result, a hybrid electrode with hierarchical structure is constructed as the cathode of solid oxide fuel cells. Compared with the single-phase $Ca_3Co_2O_6$ bulk cathode and common $Ca_3Co_2O_6$-$Ce_{0.8}Sm_{0.2}O_{1.9}$ composite one, this hybrid electrode is very active for oxygen reduction reaction. At 800 °C, area specific resistance with this cathode is reduced to 0.062 Ωcm^2, and power density peak with the electrolyte-supported single-cell is promoted to 760 mW/cm^2. The superior catalytical activity is attributed to the enlarged area for surface oxygen exchange kinetics and enhanced ionic transport behaviour.

Key words: *solid-oxide fuel cells, cathode, fiber, oxygen reduction reaction, area specific resistance*

Introduction

Sizeable impedance in solid oxide fuel cells (SOFC) arises from the catalytic cathode on which oxygen reduction reaction (ORR) is sluggish due to the hard splitting of molecular oxygen, fig. 1. Especially at the reduced operating temperatures, the cathode even becomes the main cause of polarization losses resulted from the sharply degraded activity [1-3]. So it is quite important to develop the active electro-catalysts with well-balanced physicochemical properties and to construct the appropriate electrode architectures as well.

Recently, a promising cathode material was explored to a great length by our team, and this interesting material is the hexagonal $Ca_3Co_2O_6$ (CCO) compound which shows the relatively low thermal expansion coefficient [4]. However, our subsequent investigation reveals that this material also poses the great challenges. Firstly, its ionic transport or its electronic conductivity is unreliable due to its hexagonal stacking nature of atomic arrays. Secondly, working as conventional bulk cathode constructed from the screen-printing common catalyst-containing slurry and subsequent sintering treatment, its apparent catalytic activity is barely satisfactory compared with those common cubic or quasi-cubic ABO_3-type counterparts, such as (La,Sr)$CoO_{3-\delta}$, $Ba_{0.8}Sr_{0.2}Co_{0.8}Fe_{0.2}O_{3-\delta}$, *et al* [5-8].

* Corresponding author's, e-mail: lifushao@126.com; chengfx2010@163.com

To overcome these drawbacks with CCO cathode, great effort has been devoted in our previous work and consequently the CCO's electrochemical performance is partially improved by ion doping or by making composite with other cobalt-contained perovskites [9-11]. Especially, to improve the oxygen-ion transport property, fast ion-conductor $Ce_{0.8}Sm_{0.2}O_{1.9}$ (SDC) is introduced, and accordingly a binary composite $Ca_3Co_2O_6$-$Ce_{0.8}Sm_{0.2}O_{1.9}$ (CCO-SDC) is developed by one-pot preparation [11]. However, thus prepared composite cathode presents no intentional structure which rarely conforms to the principle of efficient ORR. Firstly, in this composite structure as shown in fig. 1, SDC phase particles are too fine, and so there is insufficient bulk to form a percolating ionic conducting network. Secondly, CCO phase particles are too coarse to contribute insufficient catalytic area for surface oxygen exchange kinetics instead.

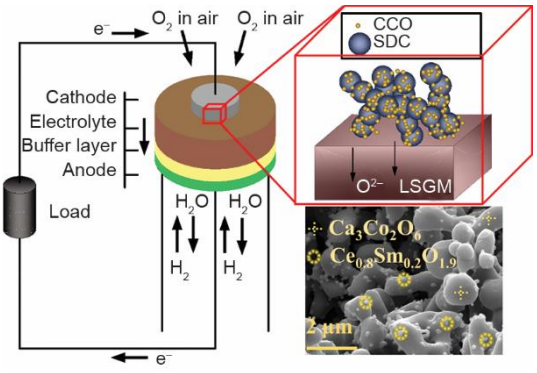

Figure 1. Components of SOFC and structure of common CCO-SDC composite cathode

To reverse that situation and to make their morphologies quite opposite, *i. e.* to make the SDC backbones much larger and to reduce CCO particles infinitely finer, herein we report a hybrid electrode with hierarchical structure as the new cathode materials of SOFC so that more marginal performance can be further gained from CCO. In this structure, high speed 3-D SDC backbones for oxygen-ion transport is first built by sintering the annealed SDC silks, and CCO nanoparticles with high specific surface are then filled in by ion-infiltration. This hybrid electrode bears much favorable catalytic activity for rapid ORR. Not confined to this function in SOFC, the designed hybrid electrode structure can also be readily applicable to other energy and environmental fields, including catalytic converters, oxygen-separation membranes, and batteries.

Experimental

Cells fabrication

As the preliminary materials, single-phase CCO powders and CCO-SDC common composite in optimized molar ratio of 1:1 are synthesized one after another according to our previous work [11]. Single-phase SDC powders and $La_{0.8}Sr_{0.2}Ga_{0.83}Mg_{0.17}O_{3-\delta}$ (LSGM) dense electrolyte discs are prepared by the sol-gel route and solid reaction respectively, as described elsewhere [12]. The SDC fibers are annealed from SDC silks at 700 ºC for 5 hours in air, which are prepared by electrospinning 0.4 N $Ce_{0.8}Sm_{0.2}(NO_3)_{3.8}$ ethanol solution with 10 wt.% polyvinyl-pyrrolidone (PVP), as sketched in fig. 2.

Button-sized single cells are fabricated, fig. 1, in which three types of cathode with different structures are successively constructed. These cathodes are the hierarchical hybrid, common composite and conventional single-phase ones, labeled as CCO@SDC, CCO-SDC, CCO, respectively. To construct CCO@SDC cathode, 3-D SDC backbones are firstly built on LSGM discs (~230 μm thick) by sintering (at 1200 ºC for 2 hours in air) the annealed SDC silks, and CCO nanoparticles are then filled in by repeatedly infiltrating 0.1 N $3Ca(NO_3)_3 \cdot 2C_4H_6CoO_4 \cdot 10C_6H_8O_7$ (citric acid) solution into SDC backbones under capillary force

and subsequent annealing at 960 ºC for 5 hours in air. Common CCO-SDC composite and conventional CCO single-phase cathodes are constructed as our previous work [11]. The anode (~30 μm thick) is constructed before cathode by screen-printing the NiO-SDC slurry onto the SDC buffer layer and subsequently baking at 1250 ºC for 4 h, whereas SDC buffer layer (~10 μm thick) is prepared by screen-printing SDC slurry onto LSGM disc and sintering at 1300 ºC for 2 hours in air.

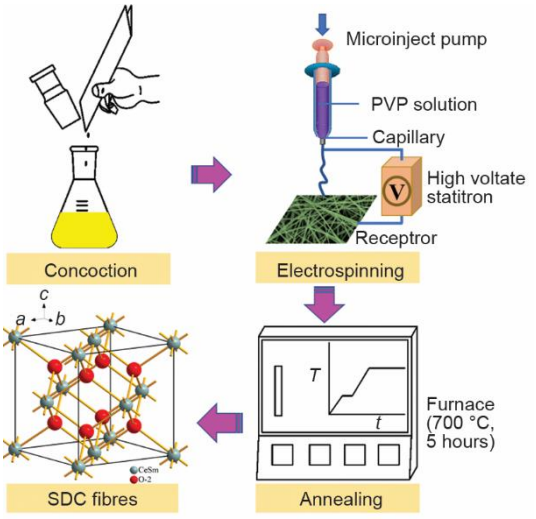

Figure 2. Preparation route for SDC fibers

Characterization and performance

Phase species are distinguished by X-ray powder diffraction (XRD, PANalytical B. V.: Empyrean) in Bragg-Brentano geometry with Cu-Ka radiation. Diffraction patterns are collected in the 2θ range of 10-80º with the scan rate of 5º per minute. Microstructural morphologies are observed by SEM, (FEI: Sirion 200) and TEM (FEI: Tecnai G2 F30).

Electrochemical impedance spectroscopy (EIS) with symmetric cells in configuration of cathode|LSGM|cathode is tested under open-circuit conditions by advanced electrochemical system (Princeton Applied Research: PARSTAT 2273). In EIS test, a sinusoidal disturbance signal with 10 mV amplitude is applied and the frequency is modulated from 100 kHz to 10 mHz, and software ZsimpWin is used to construct the equivalent circuit model and to fit the EIS data based on the least-squares method. Current-Voltage (*I-V*) curve is measured on the button-sized single cells in configuration of anode|SDC|LSGM|cathode to demonstrate the power density output and polarization extent.

Results and discussion

Figure 3 is the morphology of SDC fibers before they are applied to build 3-D cathode backbones on LSGM electrolyte discs. As shown in figs. 3(a) and 3(b), uniform and smooth SDC silks are achieved from electrospinning, and they are around 500 nm in diameter. Even after these silks are annealed and shrank greatly after cubic phase formation, the filamentous shape is still quite preserved and annealed SDC silks are turned to around 200-300 nm in diameter, as exhibited in fig. 3(c). By probing with TEM in fig. 3(d), the annealed SDC silks are found much dense and solid, and this structure is much preferred because only in this case ionic transport is consecutive after molecular oxygens are reduced to oxygen ions.

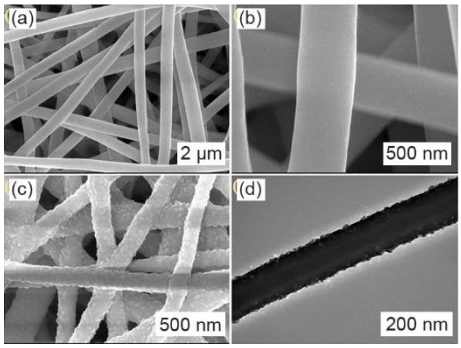

Figure 3. Morphology of SDC fibers; (a, b) SEM for fresh silks from electrospinning, (c) SEM for annealed silks, (d) TEM for annealed silks

The annealed SDC silks are further built on LSGM discs by sintering the pasted SDC fibers,

and thus 3-D backbones are constructed as fig. 4(a), firmly connected with LSGM electrolyte and greatly inherited the precursors' fibrous morphology. By comparison with common backbone built from plain SDC particles in fig. 4(b), 3-D backbones bear more favored 3-D interconnected pores, which necessarily facilitate subsequent CCO infiltration and are capable of loading more flexible amount of CCO nanoparticles. Figure 4(c) shows the hierarchical structure of CCO@SDC hybrid after infiltration of CCO into the 3-D SDC backbones. Electrocatalyst nanoparticles are very fine and large specific surface for surface oxygen exchange is generated. Meanwhile, the gaseous diffusion paths are also maintained as the unoccupied voids. By XRD identification in which the X-rays are shed directly onto the intact cathode layer, the 3-D backbones are highly compatible with the CCO, and there is no phase reaction between them, as has been well demonstrated in our preceding work [11]. No impurity phases are involved in, and LSGM diffraction peaks come from the electrolyte substrate.

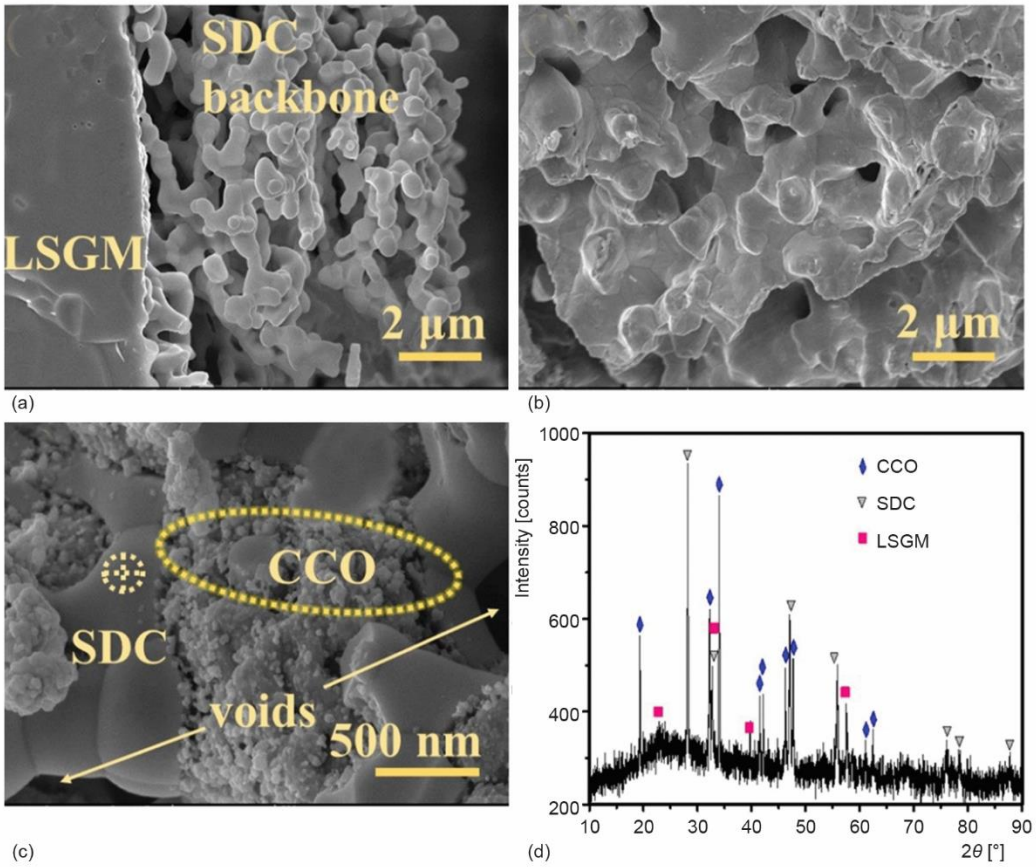

Figure 4. Structure analysis; (a) sectional SEM for SDC backbones from sintering the annealed SDC silks, (b) sectional SEM for SDC backbones from sintering the common SDC powders, (c, d) sectional SEM for CCO@SDC cathode and the corresponding XRD spectrum

Kinetics of ORR is investigated by EIS with symmetrical cathode|LSGM|cathode cells in air, and the corresponding Nyquist plots at 800 ºC are shown in fig. 5(a). On the whole, all Nyquist plots comprise two overlapped capacitance arcs arising from different relaxation processes, which means that ORR is primarily governed by two different electrode

processes [13]. Therefore, equivalent circuit model of $LR_{ohm}(Q_1R_1)(Q_2R_2)$ is used to fit the spectra if response of inductive part at high frequencies is included in, and this inductive part is frequently resulted from larger perturbation amplitude which induces large magnetic fields [14]. In this model, R_{ohm} is the ohmic resistance from the electrolyte, electrode, and lead; Q_1 and Q_2 are constant phase elements. The high-frequency resistance is associated with the charge-transfer process, R_1, while the one at low frequency is ascribed to the oxygen surface process, R_2, including oxygen adsorption-desorption of oxygen, oxygen dissociation, and surface diffusion of intermediate oxygen species [15]. The detailed fitting data are listed in tab. 1, and the fitted results agree well with the experimental measurement, and so the kinetics explanation of electrode process based on equivalent circuit is well grounded. Particularly, the length between real axes intercepts of capacitance arcs (also R_1+R_2) stands for the total cathode polarization resistance, commonly normalized as area specific resistance (*ASR*), and less *ASR* corresponds to higher electro-catalytic activity. It is evident that electrochemical activity of CCO@SDC cathode is greatly promoted in contrast with the common CCO-SDC composite and the conventional single-phase bulk CCO cathode. For example, *ASR* is only 0.062 Ω cm^2 for CCO@SDC as compared sharply with the 0.12 Ω cm^2 for CCO-SDC and the 0.28 Ω cm^2 for CCO. The temperature-dependence of *ASR* is linearly regressed to extract the thermal-activated energies, E_a, shown in fig. 5(b). Remarkably, CCO@SDC cathode exhibits a very low E_a values of 89.4 kJ/mol for the ORR (equivalent to 0.89 eV), much less than other two types of cathode. More significantly, both *ASR* and E_a of CCO@SDC cathode under comparable conditions are smaller than those of most promising ABO_3-based cathodes, as concluded in tab. 2.

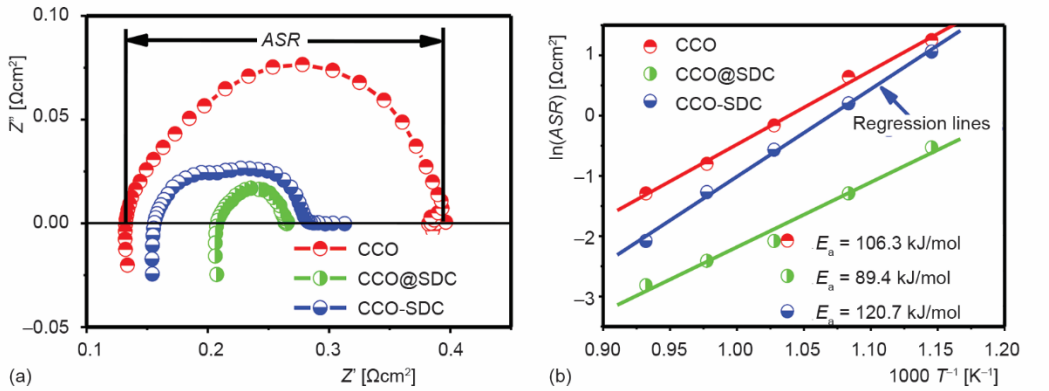

Figure 5. The EIS with different symmetrical cathodes, (a) Nyquist plots at 800 °C, (b) Arrhenius plots of temperature-dependent ASR of the electrodes and calculated active energy, E_a

Figure 6 compares the output performance of LSGM-electrolyte-supported single-cells with different cathodes. All open circuit voltages (OVC) of cells reach to high above 1.12 V, and the nearly linear *I-V* plots imply that substantial portion of the driving power is applied by the thick LSGM electrolyte. Even so, power density peaks for the cell with CCO@SDC cathode still reach to 760 mW/cm^2, 280 mW/cm^2 at 800 ºC, 650 ºC, respectively, much higher than 650 mW/cm^2 and 240 mW/cm^2 of cell with CCO-SDC cathode, further higher than 406 mW/cm^2 and 140 mW/cm^2 of cell with CCO cathode. This performance rank agrees well with that concluded from comparison of their *ASR*.

Table 1. Fitted results of EIS by $LR_{ohm}(Q_1R_1)(Q_2R_2)$ equivalent circuit with different symmetric electrodes at 800 °C

Elements	CCO	CCO-SDC	CCO@SDC
L [H]	$3.316\cdot10^{-8}$	$4.451\cdot10^{-8}$	$4.139\cdot10^{-8}$
R_{ohm} [Ω]	subtracted	subtracted	subtracted
Q_1 [$Ss^{-n}cm^{-2}$]	0.1066	0.5373	0.1368
Freq power n with Q_1	0.8546	0.7131	0.8537
R_1 [Ωcm^2]	0.1586	0.0817	0.02056
Q_2 [$Ss^{-n}cm^{-2}$]	$7.539\cdot10^{-2}$	$2.599\cdot10^{-2}$	0.2168
Freq power n with Q_2	0.7048	0.8658	0.5823
R_2 [Ωcm^2]	0.0999	0.0435	0.0398

Table 2. The *ASR* and E_a values of CCO@SDC against typical ABO_3-based cathodes on the same platform of LSGM electrolyte

Cathode	Temperatures [°C]	*ASR* [Ωcm^2]	E_a [eV]	Reference
$La_{0.6}Sr_{0.4}Fe_{0.8}Co_{0.2}O_{3-\delta}$-$Gd_{0.2}Ce_{0.8}O_{1.9}$	800	0.11	0.66	[8]
$SrCo_{0.9}Mo_{0.1}O_{3-\delta}$	750	0.13	1.05	[16]
$Sr_{0.7}Y_{0.3}CoO_{2.65-\delta}$	800	0.11	1.46	[17]
$PrBa_{0.5}Sr_{0.5}Co_{1.5}Fe_{0.5}O_{5+\delta}$	800	0.07	/	[18]
CCO@SDC	800	0.062	0.89	this work
	750	0.09		

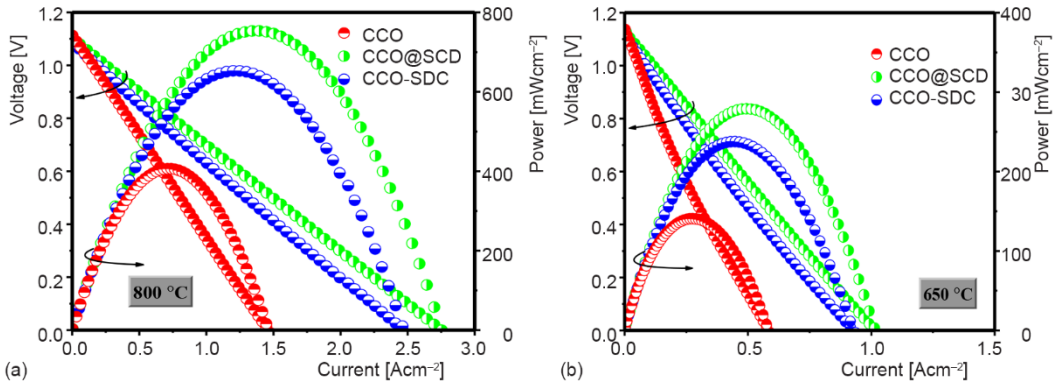

Figure 6. Current-dependent cell-voltage and power with different types of cathode at (a) 800 °C and (b) 650 °C

Conclusion

We demonstrate that CCO@SDC hierarchical hybrid is a quite promising high-performance cathode for SOFC operating below 800 °C. At 800 °C, the power density peak is around 760 mW/cm^2 for the LSGM-electrolyte-supported single-cell built with the CCO@SDC cathode, and ASR for this cathode is as low as 0.062 Ωcm^2, showing the fast ki-

netics for ORR. Meanwhile, this cathode also exhibits much favorably low active energy for ORR. We believe that much marginal performance of CCO is still left behind this novel electrode architecture because many substructures are far from being optimized, such as concentration of CCO nanoparticles, trunk size and pore distribution of SDC backbones, thickness of overall cathode layer, *etc.* The macromolecular electrospinning [19-21] and the bubble electrospinning [22-24] provide additional approach to fabrication of SDC fibers.

Acknowledgment

This work is sponsored by the Natural Science Foundation of China (Grants 51632001 and 51764048). The authors are grateful to Shanghai Key Laboratory of Rare Earth Functional Materials for financial support.

References

[1] Zhang, Y., *et al.*, Recent Progress on Advanced Materials for Solid-Oxide Fuel Cells Operating Below 500 °C, *Advanced Materials*, *29* (2017), 48, ID 1700132
[2] Zhu, Y., *et al.*, Promotion of Oxygen Reduction by Exsolved Silver Nanoparticles on a Perovskite Scaffold for Low-Temperature Solid Oxide Fuel Cells, *Nano Letters*, *16* (2016), 1, pp. 512-518
[3] Jun, A., *et al.*, Perovskite as a Cathode Material: A Review of Its Role in Solid-Oxide Fuel Cell Technology, *ChemElectroChem*, *3* (2016), 4, pp. 511-530
[4] Wei, T., *et al.*, Evaluation of $Ca_3Co_2O_6$ as Cathode Material for High-Performance Solid-Oxide Fuel Cell, *Scientific Reports*, *3* (2013), Jan., ID 1125
[5] Zhou, W., *et al.*, A Highly Active Perovskite Electrode for the Oxygen Reduction Reaction Below 600 °C, *Angewandte Chemie International Edition*, *52* (2013), 52, pp. 14036-14040
[6] Shao, Z., *et al.*, A High-Performance Cathode for the Next Generation of Solid-Oxide Fuel Cells, *Nature*, *431* (2004), 7005, pp. 170-173
[7] Dieterle, L., *et al.*, Microstructure of Nanoscaled $La_{0.6}Sr_{0.4}CoO_{3-\delta}$ Cathodes for Intermediate-Temperature Solid Oxide Fuel Cells, *Advanced Energy Materials*, *1* (2011), 2, pp. 249-258
[8] Gong, Y., *et al.*, Atomic Layer Deposition Functionalized Composite SOFC Cathode $La_{0.6}Sr_{0.4}Fe_{0.8}Co_{0.2}O_{3-\delta}$-$Gd_{0.2}Ce_{0.8}O_{1.9}$: Enhanced Long-Term Stability, *Chemistry of Materials*, *25* (2013), 21, pp. 4224-4231
[9] Li, F., *et al.*, One-Pot Synthesized Hetero-Structured $Ca_3Co_2O_6$/$La_{0.6}Ca_{0.4}CoO_3$ Dual-Phase Composite Cathode Materials for Solid-Oxide Fuel Cells, *International Journal of Hydrogen Energy*, *40* (2015), 37, pp. 12750-12760
[10] Li, F., *et al.*, Evaluation of $Ca_3(Co,M)_2O_6$ (M = Co, Fe, Mn, Ni) as New Cathode Materials for Solid-Oxide Fuel Cells, *Progress in Natural Science: Materials International*, *25* (2015), 5, pp. 370-378
[11] Li, F., *et al.*, $Ca_3Co_2O_6$-$Ce_{0.8}Sm_{0.2}O_{1.9}$ Composite Cathode Material for Solid Oxide Fuel Cells, *Journal of Alloys and Compounds* , *753* (2018), July, pp. 292-299
[12] Huang, Y. H., *et al.*, Double Perovskites as Anode Materials for Solid-Oxide Fuel Cells, *Science*, *312* (2006), 5771, pp. 254-257
[13] Murray, E. P., *et al.*, Oxygen Transfer Processes in (La,Sr)MnO_3/Y_2O_3-Stabilized ZrO_2 Cathodes: An Impedance Spectroscopy Study, *Solid State Ionics*, *110* (1998), 3-4, pp. 235-243
[14] Klotz, D., *et al.*, Practical Guidelines for Reliable Electrochemical Characterization of Solid Oxide Fuel Cells, *Electrochimica Acta*, *227* (2017), 227, pp. 110-126
[15] Zhou, W., *et al.*, A New Cathode for Solid Oxide Fuel Cells Capable of In Situ Electrochemical Regeneration, *Journal of Materials Chemistry*, *21* (2011), 39, pp. 15343-15351
[16] Aguadero, A., *et al.*, A New Family of Mo-doped $SrCoO_{3-\delta}$ Perovskites for Application in Reversible Solid State Electrochemical Cells, *Chemistry of Materials*, *24* (2012), 14, pp. 2655-2663
[17] Li, Y., *et al.*, Oxygen-Deficient Perovskite $Sr_{0.7}Y_{0.3}CoO_{2.65-\delta}$ as a Cathode for Intermediate-Temperature Solid Oxide Fuel Cells, *Chemistry of Materials*, *23* (2011), 22, pp. 5037-5044
[18] Jiang, L., *et al.*, Thermal and Electrochemical Properties of $PrBa_{0.5}Sr_{0.5}Co_{2-x}Fe_xO_{5+\delta}$ (x = 0.5, 1.0, 1.5) Cathode Materials for Solid-Oxide Fuel Cells, *Journal of Power Sources*, *232* (2013), June, pp. 279-285
[19] Tian, D., He, J. H., Macromolecular Electrospinning: Basic Concept & Preliminary Experiment, Results in Physics, *11* (2018), Dec., pp. 740-742
[20] Tian, D., *et al.*, Macromolecule Orientation in Nanofibers, *Nanomaterials*, *8* (2018), 11, ID 918

[21] Tian, D., *et al.*, Self-Assembly of Macromolecules in a Long and Narrow Tube, *Thermal Science, 22* (2018), 4, pp. 1659-1664
[22] Li, Y., He, J. H. Fabrication and Characterization of ZrO_2 Nanofibers by Critical Bubble Electrospinning for High-Temperature-Resistant Adsorption and Separation, *Adsorption Science & Technology, 37* (2019), 5-6, pp. 425-437
[23] Peng, N. B., *et al.*, A Rachford-Rice-Like Equation for Solvent Evaporation in the Bubble Electrospinning, *Thermal Science, 22* (2018), 4, pp. 1679-1683
[24] Zhou, C. J., *et al.*, Silkworm-Based Silk Fibers by Electrospinning, *Results in Physics, 15* (2019), Dec., ID 102646

Paper submitted: April 24, 2019
Paper revised: September 29, 2019
Paper accepted: September 29, 2019

© 2020 Society of Thermal Engineers of Serbia.
Published by the Vinča Institute of Nuclear Sciences, Belgrade, Serbia.
This is an open access article distributed under the CC BY-NC-ND 4.0 terms and conditions.